Optical Properties of Sub-Wavelength Dielectric Gratings and their Application for Surface Enhanced Raman Scattering

Min Hu, David Fattal, Jingjing Li, Xuema Li, Stanley R. Williams, Zhiyong Li

HP Laboratories
HPL-2011-17

Keyword(s):

Sub-wavelength grating, surface enhanced Raman, dispersion relation

Abstract:

We fabricated and measured the far-field optical properties of a sub-wavelength Si3N4 (silicon nitride) two dimensional grating. Frequency-dependent transmission measurements from a white-light source revealed that both transverse magnetic (TM) and transverse electric (TE) modes were excited on the grating. We determined the dispersion relations of the modes by tilting the sample with respect to the incoming light beam and measuring the frequency shift of the absorption features. By comparing to a simple model, we determined the effective refractive index for the TM and TE modes and the geometrical constants for the grating. This information enables gratings with desired optical properties to be designed and fabricated. The application of the sub-wavelength grating for surface enhanced Raman scattering (SERS) is demonstrated.

External Posting Date: February 6, 2011 [Fulltext] Approved for External Publication
Internal Posting Date: February 6, 2011 [Fulltext]

Optical Properties of Sub-Wavelength Dielectric Gratings and their Application for Surface Enhanced Raman Scattering

Min Hu,[†*] David Fattal,[†] Jingjing Li,[†] Xuema Li,[†] R. Stanley Williams,[‡] Zhiyong Li[*]

[†]*Intelligent Infrastructure Lab, Hewlett-Packard Laboratories, 1501 Page Mill Road, Palo Alto, CA 94304 USA* [‡]*Memristor Research Group, Hewlett-Packard Laboratories, 1501 Page Mill Road, Palo Alto, CA 94304 USA*

Abstract

We fabricated and measured the far-field optical properties of a sub-wavelength Si_3N_4 (silicon nitride) two dimensional grating. Frequency-dependent transmission measurements from a white-light source revealed that both transverse magnetic (TM) and transverse electric (TE) modes were excited on the grating. We determined the dispersion relations of the modes by tilting the sample with respect to the incoming light beam and measuring the frequency shift of the absorption features. By comparing to a simple model, we determined the effective refractive index for the TM and TE modes and the geometrical constants for the grating. This information enables gratings with desired optical properties to be designed and fabricated. The application of the sub-wavelength grating for surface enhanced Raman scattering (SERS) is demonstrated.

[*] Corresponding authors: M. Hu (min.hu@hp.com) and Z. Li (zhiyong.li@hp.com)

Grating structures have drawn intensive research interest since the observation of extraordinary optical transmission from a sub-wavelength hole-array grating in a silver thin film.[1] Continued research has led to a number of applications, such as surface enhanced Raman scattering (SERS) sensing, based on the unique optical resonance properties and the spatial confinement of the electromagnetic (EM) field.[2,3,4] An analogue of this optical property, the Guided-Mode Resonance (GMR),[5] exists in dielectric gratings, which has a much higher quality factor (Q) because of the lower absorption compared to metals. This high Q property of dielectric gratings has led to interesting applications, such as narrow band optical filters.[6,7,8,9,10] However, dielectric gratings can also be used as a field enhancement element, since a GMR provides a very strong local electric field when properly excited.[11,12] Recently, a theoretical study has shown that a local electric field enhancement can be achieved for a hole-array dielectric grating.[13] In this letter, we report the fabrication of a sub-wavelength dielectric grating and the experimental verification of GMRs excited on the grating by far-field tilt-angle dependent measurements of the spectrum of transmitted white light. We identified TM and TE modes, mapped the dispersion relations of both types, and used this information to determine important physical and geometrical parameters of the grating that can be used to design new gratings with desired GMRs. Finally we will show the SERS application of our sub-wavelength grating structures based on excitation of GMRs.

Our design of the dielectric grating was based on our previous theoretical simulation.[13] A two dimensional array of square holes with a nominal width of 233 nm and a periodicity of 465 nm

was etched partially into a silicon nitride film on a silicon dioxide substrate to form the grating. The intended GMR of the grating was for an excitation wavelength of 785 nm. We fabricated the grating structure using e-beam lithography and dry etching. We started with a plasma enhanced chemical vapor deposition (PECVD) of 200 nm of low stress silicon nitride onto a fused silica substrate. The film was coated with 5 nm Cr by e-beam evaporation and then 100 nm PMMA by spin coating for e-beam lithography. After the e-beam pattern was developed on the PMMA layer, the thin Cr layer was removed by a wet etchant. Reactive ion etching with CF_4/H_2 was used to etch 50 nm deep holes into the silicon nitride using PMMA as the etching mask. After the etching process, the sample was cleaned with acetone, Cr etchant, and a piranha cleaning step to remove any residual polymers on the sample. Representative scanning electron microscope (SEM) and atomic force microscope (AFM) images of the grating structure are shown in Figure 1a and 1b, respectively. Slightly distorted square holes can be seen in the images shown in Figure 1. The period of the grating was measured to be 471 ± 2 nm in the '*x*' direction and 436 ± 2 nm in the '*y*' direction, which differed from the designed grating period (465 nm) because of calibration drift of the SEM used for the electron beam lithography. The depth of the square holes on the grating was extracted from the cross-sectional profile across the holes in the AFM image. The inset of Figure 1b reveals that the actual etched depth matched the designed value (50 nm) fairly well.

A purpose-built micro-spectrograph was employed to characterize the transmission characteristics of the grating. The experimental measuring system we used in this work is depicted in Figure 1c. Briefly, a halogen lamp was used as the broad band illumination source,

and a pinhole-lens combination was used to collimate the incident light so that we have an approximately plane-wave beam. We controlled the polarization of the incident light using a linear polarizer. The grating was placed on the stage of an inverted microscope with freedom to tilt, and a 20× objective (N.A. 0.25) was used to collect the transmitted light underneath the grating structure. The collected light was then dispersed through a spectrograph and recorded by an imaging charge coupled device (CCD). To collect the transmission spectra, we first locate the area of interest using dark-field epi-illumination because of better image contrast of the grating. The zero order of the spectrograph dispersive grating was used to image the sample on the CCD in order to define a collection area. Once the collection area was fixed, we switched from the dark-field epi-illumination to a bright-field illumination from a top light source, and moved the spectrograph to the wavelength of interest. A schematic drawing of the grating sample from side view and a dark-field real color image of the grating sample (100 μm×100 μm hole array top view) are shown in Figure 1c.

We controlled the polarization of the illumination light by inserting a linear polarizer in the optical path so that the polarization of the incident light can be aligned either along the *x* or *y* direction shown in Figure 1c. The grating sample remained at 0° incident angle (normal incidence) and the measured transmission spectra were shown in Figure 1d. A polarization aligned with *x* axis (blue trace in Figure 1d) led to resonances at 715 nm and 755 nm, while the *y* polarization (red trace in Figure 1d) resulted in resonances at 700 nm and 775 nm. Based on the simulation results, these two groups of resonance with the polarization of illumination along *x* and

y should overlap with each other if the grating has a perfect square geometry, i.e., $\Lambda_x = \Lambda_y$, where Λ_x and Λ_y are the periodicities of the grating along *x* and *y* direction, respectively. However, we observed a slight mismatch for the transmission peaks between *x* and *y* polarizations. This discrepancy is not a surprising result and it possibly stems from the anisotropic grating dimensions ($\Lambda_x \neq \Lambda_y$) as seen in the SEM image (Figure 1a). Therefore, a larger periodicity along *x* would produce a TE resonant wave, which propagated along *x*, at longer wavelength under *y*-polarized light (see discussion in the following text).

We further studied the angular dependence of the resonance by tilting the grating at small angle intervals, for example, every 1 or 2 degrees, under both *p* and *s* polarized illumination. Figure 2a,d and 2b,e show the top view (a dark field microscopy image) and the side view (a schematic drawing) of the Si_3N_4 grating with regard to the tilting geometry, respectively. For *p* polarized illumination, the incident polarization was aligned with the *x* axis, therefore the magnetic component of the incident field is always parallel with the substrate while tilting the grating. The mode splitting can be clearly observed in the transmission spectra as shown in Figure 2c as we increased the tilting angles. In this case, the resonance at 755 nm remained almost unchanged in spectral position at small tilting angles (no angular dependence), but the degeneracy of the other resonance at 715 nm was split, with one mode shifting to shorter wavelength while the other shifting to longer wavelength with increasing tilt angle. This phenomenon can be understood as follows. Under normal incident condition, the incident light wave launched four propagating waves along ± *x* and ± *y* directions. In the configuration

shown in Figure 2a, the waves along ±x direction were TM modes while the other two along ±y directions were TE modes. When a p polarized incidence is applied to the waveguide as shown in Figure 2a and 2b, the resonance of the TE related mode should remain fixed because the magnetic field was unperturbed. However, the resonance of the TM related mode was expected to have a symmetric splitting behavior due to the varying projected component of the electric field strength with regard to the tilting angles. Specifically, the resonant condition of the TM mode that propagates along ±x direction can be roughly described as:

$$k_{TM} = \frac{2\pi}{\Lambda_x} \pm k_x = \frac{2\pi}{\Lambda_x} \pm k_0 \sin\theta \tag{1}$$

where k_{TM} is the propagating constant of the TM guided mode along ±x direction, k_0 is the wavenumber of the incident wave in free space, and θ is the angle of incidence. When θ=0, the structure goes to resonance when the period Λ_x=2π/k_{TM}, which gives the single TM mode peak around 715 nm for the normal incidence (spectrum at 0° in Fig. 2c). However, when θ is not 0° (oblique incidence), from Eq. (1) we see that there may be two possible k_0 that would satisfy the equation associated with the + or - sign, respectively. This nonzero value will lead to a splitting behavior of the single TM peak into two peaks above and below the original peak wavelength, and these two peaks shift equal amount away from each other as the incident angle increases. Based on the above analysis, it is fairly easy to identify the longer wavelength resonance at 755 nm in Figure 2c as a TE mode and the shorter wavelength resonance at 715 nm as a TM mode. Note in Figure 2c that the longer wavelength TM mode started to mix with the TE mode to show an anti-crossing feature when the tilting angle was large enough. In the anti-crossing region (above

4°), we noticed that an additional weak mode can be seen at even longer wavelength above 800 nm. This weak mode was possibly a higher order TE mode and we will not discuss that due to the limit of the space. Similarly, in Figure 2 d-f, we observed the TE mode splitting when we chose the incident light to be *s* polarization. Again, the observed angular dependent mode splitting for the longer wavelength resonance at 775 nm was ascribed to the TE nature of the mode. The shorter wavelength resonance at 700 nm almost stays unaltered regardless of the tilting angle since it was TM related. The amount of the spectral shift was estimated to be ~7 nm per degree of tilting for both TE and TM modes. It is worth pointing out that we occasionally observed a doublet feature of the resonance peak, for example, the TM mode peaks at 1.5° and 5° in Figure 2f. This doublet is not a surprising result because the tilting of the sample may not be a perfect in-plane tilting at some angles given that the resonance is very sensitive to the angles. Secondly, a slight mis-alignment of the polarization with the grating geometry can result a splitting "doublet" in the spectra.

Finally, in Figure 3a and 3b we show the dispersion relation (k_0 vs. sinθ) of both TE and TM modes extracted from the experimental values, respectively. Assuming $k_{TM} = k_0 n_{eff}(k_0)$ where n_{eff} is the effective refractive index for the TM mode and it's a function of k_0, then we can rearrange the equation (1) for the grating to obtain a simple formula of n_{eff} for TM and TE modes:

$$n_{eff} = \frac{\lambda_0}{\Lambda_x} \pm \sin\theta \qquad (2)$$

where λ_0 is the resonance wavelength of TM mode or TE mode and $k_0=2\pi/\lambda_0$. We plot the experimentally extracted n_{eff} as a function of k_0 in Figure 3c and 3d for both modes. It is not hard

to find out that the n_{eff} are almost linearly scaled with the wavevector. For the TE mode, the n_{eff} is higher compared to the TM mode. Note the experimentally determined values of n_{eff} are reasonable given that the guided modes propagate along the interface of Si_3N_4 (n=2.05), silicon dioxide (n=1.46) and air (n=1.00). A higher n_{eff} for the TE mode possibly indicated that the TE mode is more confined in the Si_3N_4 layer compared to the TM mode.

We realized that the above mentioned optical property of the grating will be very useful for the applications that require strong field enhancement near the surface, such as the SERS. In SERS, the enhancement factor is approximately scaled with $|E_{\omega p}|^2 \cdot |E_{\omega s}|^2$, where $|E_{\omega p}|$ and $|E_{\omega s}|$ are the magnitudes of the local electric field at the pump laser frequency ω_p and the Raman scattering frequency ω_s, respectively. First, the high Q of the grating resonance is believed to improve the SERS enhancement due to the amplified local electric field resulting from the guided wave resonance. Second, the wavelength tunability as a function of the tilting angle simply means that we can choose the fixed resonance, for example, the TM mode under *s*-polarized illumination (see Figure 2f), to overlap with the pump laser frequency ω_p to achieve a maximum Raman excitation. Meanwhile, we can tune the other shifting resonance (e.g. the TE mode in Figure 2f) to match the Raman scattering frequency ω_s such that the Raman emission can be greatly improved. We believe our sub-wavelength grating structure in combination with properly designed optical antenna will provide a novel platform for SERS sensing application.

As a proof of concept, we show that our sub-wavelength gratings can be used to enhance the Raman scattering of the molecules adsorbed in close proximity to the substrate surface. We

deposited a thin metal (Au) island film with a nominal thickness of 1.5 nm, by e-beam evaporation at normal incidence, on top of our sub-wavelength grating. The thin metal film coating does not significantly change the optical resonance feature of the grating. It only changes the bandwidth slightly and does not shift the position of the GMRs (data not shown). The molecules on the Au islands can not only experience the localized surface Plasmon (LSP) of the gold islands on the grating surface but also interact with the propagating GMRs of the grating itself. We performed the Raman experiment with the trans-1,2-bis(4-pyridyl)-ethylene (BPE) molecules adsorbed on the substrate surface. A standard confocal Raman microscope (Jobin-Yvon T64000) using epi-illumination mode was employed for the Raman measurements. All spectra were collected through a 100× (N.A. 0.9) objective with the excitation of 632.8 nm and 784.5 nm. The laser power at the sample was about 2 mW for both 632.8 nm and 784.5 nm laser. The integration time was at 10s. The sub-wavelength grating substrates coated with Au were soaked in 1 mM BPE in ethanol for 10 minutes. Then the substrates were washed with copious amounts of ethanol to remove the physically attached BPE molecules and subsequently dried in a nitrogen stream prior to Raman measurement.

Figure 4(a) shows the Raman spectra of the BPE molecules with an excitation wavelength of 632.8 nm. The polarization was aligned along *y*-axis of the grating, so the Raman scattering window (680 nm-710 nm) falls into the same region of the GMR at 700 nm (see red curve in Fig. 1d). It is clear that the Raman signal was enhanced by comparing the measurements taken "on" grating areas and "off" grating areas. This enhancement is due to the amplification of the scattering part of the SERS, i.e., $|E_{\omega s}|$ as mentioned above. On the other

hand, we can also enhance the Raman by amplifying the pumping electrical field $|E_{\omega p}|$. Figure 4(b) shows the Raman spectra excited at 784.5 nm, which is very close to the GMR at 775 nm, i.e., the longer wavelength GMR of the red curve shown in Fig. 1d. In this case, the incident EM field $|E_{\omega p}|$ was amplified due to the matching of the pumping laser with the GMR. However, the Raman scattering window (860 nm-910 nm) for the BPE molecule is far away from the GMR at 775 nm. Thus, there is no obvious enhancement for the scattering field $|E_{\omega s}|$. It is worth noting that the signal strength in Figure 4(b) was slightly lower compared to Figure 4(a), this is probably because the mismatch of the localized surface plasmon resonance of the Au nanostructures with the longer wavelength of the incident laser.[14] It is more important to point out that the tunability of GMRs gives us more freedom to engineer the sub-wavelength grating structures to further enhance the Raman scattering. For example, one can tune GMRs to simultaneously align with both the incident laser wavelength and the Raman scattering window of a specific molecule.

In summary, we fabricated and characterized sub-wavelength dielectric gratings by measuring their far-field optical transmission spectra. Studies of the dispersion relation of the grating show that both TM and TE GMR modes can be excited and tuned by changing the incident angles. We integrated gold nano-structures with our sub-wavelength gratings and demonstrated that the GMRs of the grating can be very useful for SERS applications.

Acknowledgements. We acknowledge Tan Ha, Cuong Le and Alvin Stanley for assistance in the laboratory. We also thank Wei Wu, S. Y. Wang and Huei-Pei Kuo for helpful discussions.

This work was partially supported by the Defense Advanced Research Projects Agency (DARPA of the United States Department of Defense) HR0011–09–3–0002.

References:

[1] T. W. Ebbesen, H. J. Lezec, H. F. Ghaemi, T. Thio, P. A. Wolff, Nature **391,** 667 (1998)

[2] A. G. Brolo, E. Arctander, R. Gordon, B. Leathem, K. L. Kavanagh, Nano Lett. **4,** 2015 (2004)

[3] M. Hu, F. Ou, W. Wu, I. Naumov, X. Li, A. Bratkovsky, R. S. Williams, Z. Li, J. Am. Chem. Soc. **132,** 12820 (2010)

[4] M. Hu, I. Naumov, A. Bratkovsky, R. S. Williams, Z. Li, unpublished results.

[5] S. S. Wang, R. Magnusson, J. S. Bagby, J. Opt. Soc. Am. A **7,** 1470 (1990)

[6] A. Sharon, D. Rosenblatt, A. A. Friesem, J. Opt. Soc. Am. A **14**, 2985 (1997)

[7] R. Magnusson, D. Shin, Z. S. Liu, Opt. Lett. **23**, 612 (1998)

[8] Z. S. Liu, S. Tibuleac, D. Shin, P. P. Young, R. Magnusson, Opt. Lett. **23**, 1556 (1998)

[9] T. Sang, Z. Wang, L. Wang, Y. Wu, L. Chen, J. Opt. A: Pure Appl. Opt. **8**, 62 (2006)

[10] C. Wei, S. Liu, D. Deng, J. Shen, J. Shao, Z. Fan, Opt. Lett. **31**, 1223 (2006)

[11] S. M. Kim, W. Zhang, B. T. Cunningham, Appl. Phy. Lett. **93**, 143112 (2008)

[12] S. M. Kim, W. Zhang, B. T. Cunningham, Opt. Exp. **18**, 4300 (2010)

[13] J. Li, D. Fattal, Z. Li, Appl. Phy. Lett. **94**, 263114 (2009)

[14] J. Zhao, J. A. Dieringer, X. Zhang, G. C. Schatz, R. P. Van Duyne, J. Phys. Chem. C **112**, 19302, (2008)

Figure Captions:

Figure 1. (Color) SEM (a) and AFM (b) images of the Si_3N_4 dielectric grating. Inset of (b): a cross-section line profile of the grating along the red line (on the AFM image) indicating the depth of the square holes. (c) Left: a sketch of the experimental set-up to measure the far-field transmission spectrum of the grating sample, which was given a tilting freedom. Right: a sketch of the grating from side view and a large scale real color image of the grating under dark-field microscope. (d) Normal incidence transmission spectra taken with the polarization aligned with *x* direction (blue) and *y* direction (red), respectively.

Figure 2. (Color) (a)-(c): Schematics of *p* polarized illumination with the polarization along *x* axis (a and b) and the angular dependent transmission spectra of the grating (c). (d)-(f): Schematics of *s* polarized illumination with the polarization along *y* axis (d and e) and the angular dependent transmission spectra of the grating (f). The red and blue dash lines in the spectra plot are guide to eyes indicating the TM and TE mode, respectively. Red arrows indicated increased angles. (see text for details)

Figure 3. (a) and (b): Dispersion relation of the TM (red color) and TE modes (blue color) of the Si_3N_4 grating under *p* polarized (a) and *s* polarized (b) illumination. The open triangles and the solid squares are experimental values. (c) and (d): Plot of n_{eff} as a function of wavevector (k_0) for TM (c) and TE mode (d), respectively. Note different scales in (c) and (d).

Figure 4. Raman spectra of BPE molecules taken from the gold islands coated grating area (red curves) and non-grating area (blue curves) under different excitation wavelengths of 632.8 nm (a) and 784.5 nm (b). The insets in both figures are optical dark-field images of the grating. An AFM image of a local area of the grating was shown as an inset in (a). The top-right inset of (a) also shows a zoomed-in AFM image of the gold islands (scale bar = 50 nm).

Figure 1.

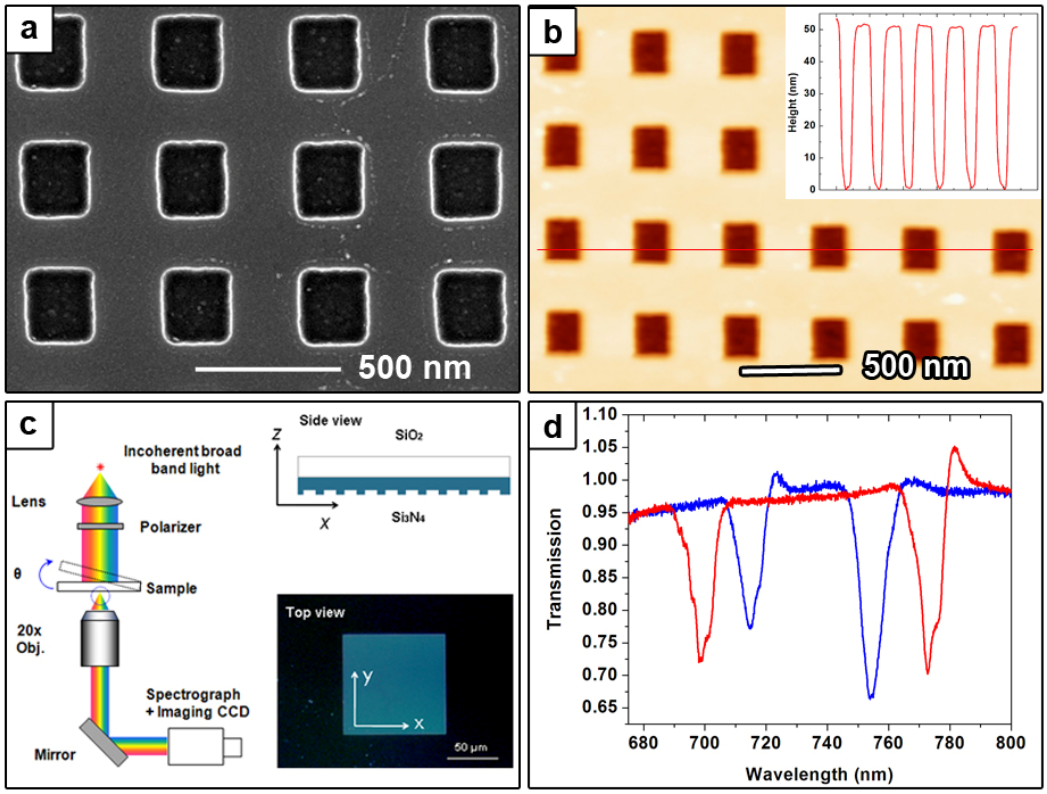
a
500 nm
b
Height (nm)
500 nm
c
Incoherent broad band light
Lens
Polarizer
θ
Sample
20x Obj.
Spectrograph + Imaging CCD
Mirror
Side view
Z
X
SiO2
Si3N4
Top view
y
x
50 μm
d
Transmission
Wavelength (nm)

Figure 2.

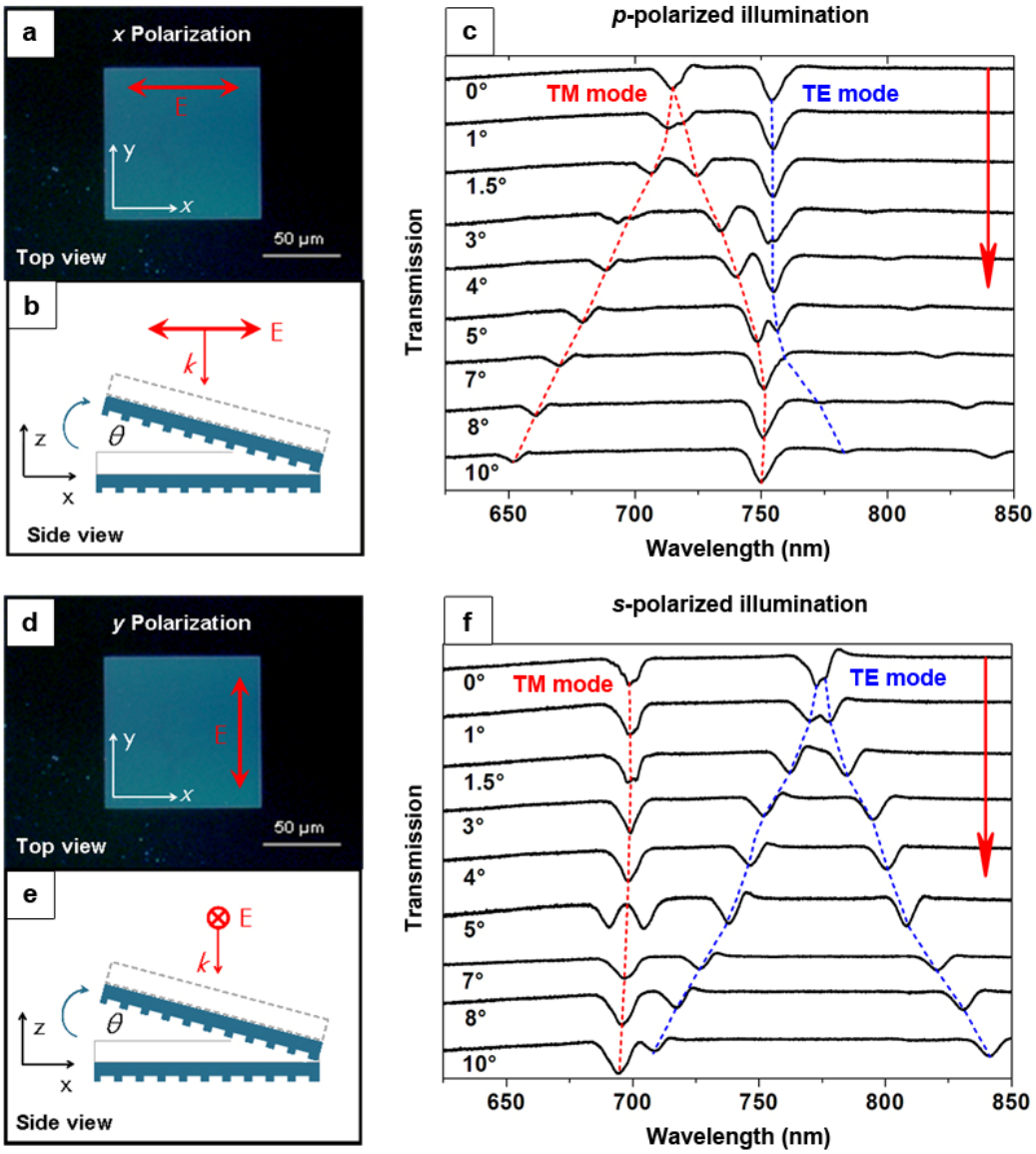
a
x Polarization
E
y
x
50 μm
Top view
b
E
k
θ
z
x
Side view
c
p-polarized illumination
0°
1°
1.5°
3°
4°
5°
7°
8°
10°
TM mode
TE mode
Transmission
650
700
750
800
850
Wavelength (nm)
d
y Polarization
E
y
x
50 μm
Top view
e
E
k
θ
z
x
Side view
f
s-polarized illumination
0°
1°
1.5°
3°
4°
5°
7°
8°
10°
TM mode
TE mode
Transmission
650
700
750
800
850
Wavelength (nm)

Figure 3.

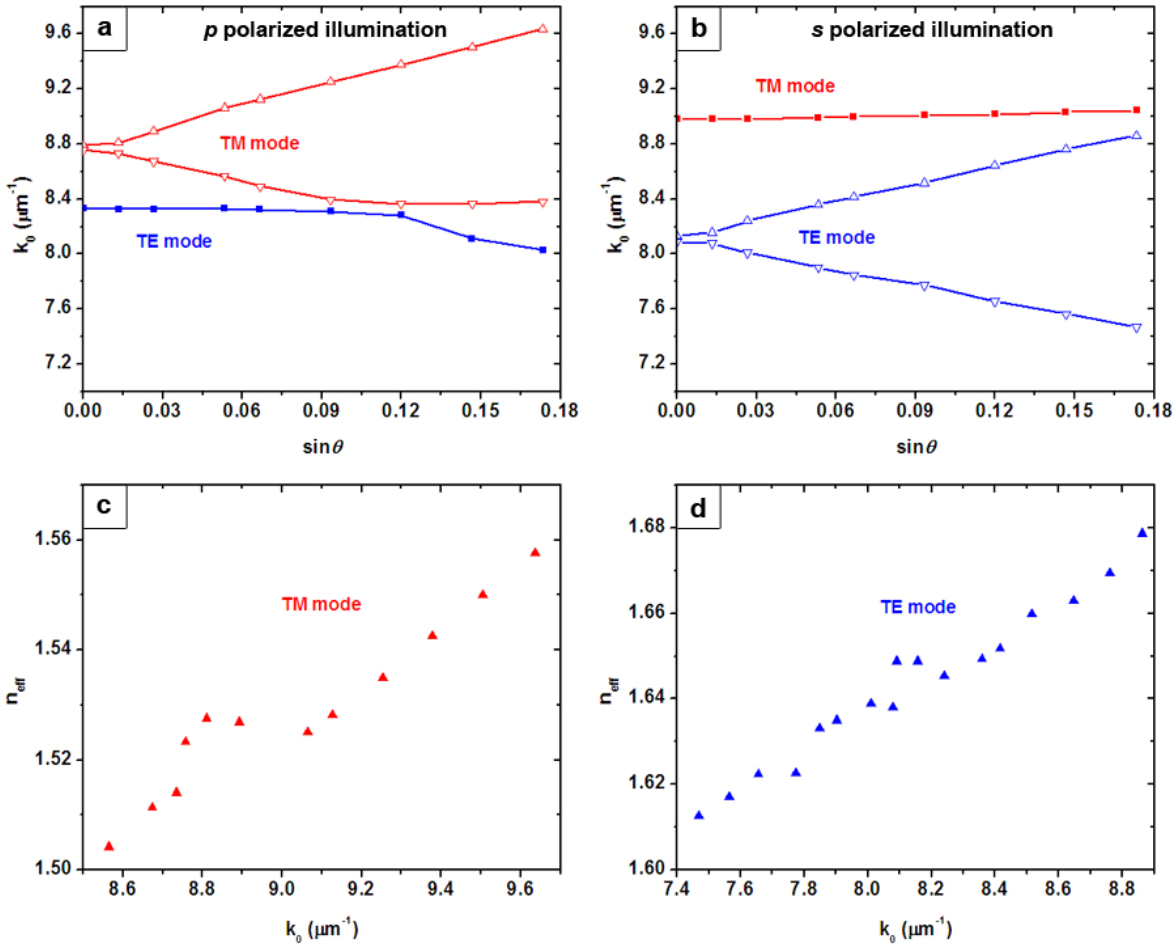
a
p polarized illumination
TM mode
TE mode
k0 (μm-1)
sinθ
b
s polarized illumination
TM mode
TE mode
k0 (μm-1)
sinθ
c
TM mode
neff
k0 (μm-1)
d
TE mode
neff
k0 (μm-1)

Figure 4.

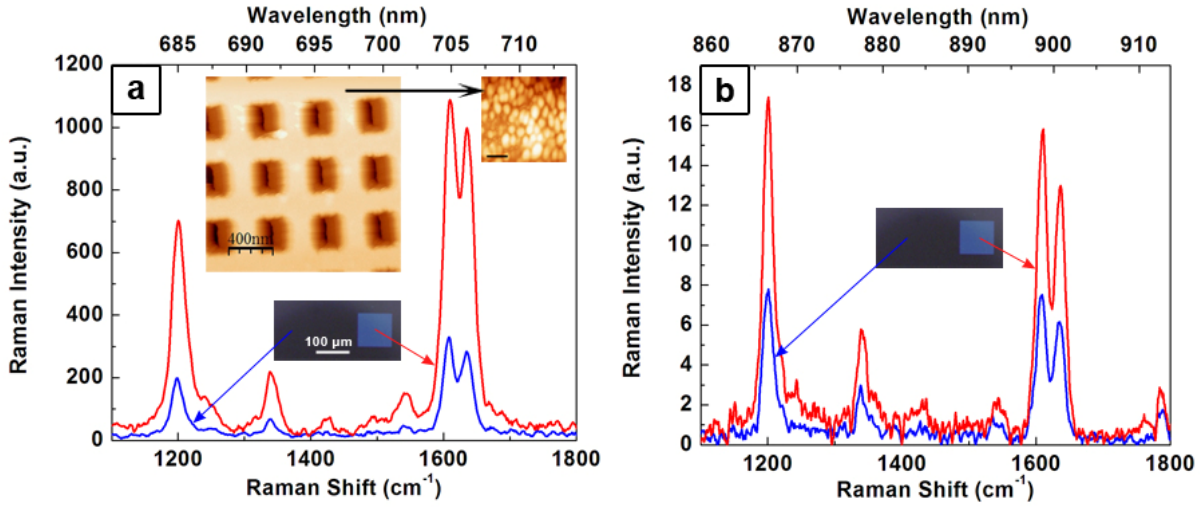
a
Wavelength (nm)
685 690 695 700 705 710
1200 1000 800 600 400 200 0
Raman Intensity (a.u.)
400nm
100 μm
1200 1400 1600 1800
Raman Shift (cm-1)
b
Wavelength (nm)
860 870 880 890 900 910
18 16 14 12 10 8 6 4 2 0
Raman Intensity (a.u.)
1200 1400 1600 1800
Raman Shift (cm-1)